nature electronics

Article

https://doi.org/10.1038/s41928-025-01516-w

Body sensor networks based on flexible topological clothing

Received: 27 January 2025

Accepted: 4 November 2025

Published online: 5 January 2026

Check for updates

Zhipeng Li[1,2,9], Zhu Liu[3,9] ✉, Zhen Wang[3], Yikuan Deng[3], Shuihua Yang[2], Jianfeng Chen[2], Qihang Zeng[2], Yuzhe Zhong[4], Haitao Yang[4], Ze Xiong[5], Xi Tian[6], Gaosheng Li[7], Yang Chen[8], Hui Jing[3] ✉, John S. Ho[2] & Cheng-Wei Qiu[2] ✉

Body sensor networks wirelessly interconnect multiple on-body sensors using metamaterials that are capable of supporting microwave near-field or surface-wave propagations. However, the design of such networks is typically restricted to one-dimensional unit-cell structures. Topological metamaterials are often used in photonics applications such as lasers and photon sources, but their integration with biological systems remain limited due to low flexibility, high bending loss and high energy dissipation in biological environments. Here we report flexible topological metamaterial clothing that can provide robust biosensing networks on the human body. The approach is based on two-dimensional topological modules fabricated from thin metallic conductive textiles. The resulting topological edge states improve on-body signal transmission by over three orders of magnitude (more than 30 dB) compared with conventional radiative networks, and can maintain performance under various bending angles. The modular design allows reconfiguration by varying the combination of topological phase modules. We show that the topological clothing with interconnected biosensors, and enhanced with machine learning algorithms, can monitor vital signs during exercise with an over two orders of magnitude improvement in signal-to-noise ratio and a threefold increase in accuracy compared with a system without topological clothing.

The topology degree of freedom is of use in wave manipulation, providing capabilities that lie beyond conventional device designs[1–5]. Governed by symmetry-protected topological order, topological devices feature non-trivial bands and topological boundary modes[6–8]. These designs are commonly used in photonic metamaterials, unlocking exotic wave phenomena such as robust, defect and disorder-immune waveguiding[9–11] and offer practical applications in lasers and photon sources[12–16]. However, the integration of topological metamaterials with biological systems, particularly the human body, remains limited due to challenges such as low device flexibility, high bending loss and high energy dissipation in biological environments[17,18].

Flexible interfaces between metamaterials and biological systems could, however, be of use in healthcare technologies[19]. Of particular interest are body sensor networks, which wirelessly interconnect multiple on-body biosensors using metamaterials capable of supporting microwave near-field or surface-wave propagations[20–22]. The networks are energy efficient and resistant to eavesdropping, and demonstrated improved sensing performance compared with single-node systems, enabling multi-vital-sign monitoring and closed-loop therapies[23–25]. However, the design of sensor networks commonly relies on one-dimensional unit-cell structures such as coil relays or spoof surface plasmon waveguides[22–28].

In this Article, we report flexible topological clothing that provides robust biosensor networks for vital-sign monitoring during exercise. We design the topological clothing using a planar valley topological model and fabricate two modules with opposite-signed

A full list of affiliations appears at the end of the paper. ✉e-mail: zhu_liu@hnu.edu.cn; jinghui@hunnu.edu.cn; chengwei.qiu2@nus.edu.sg

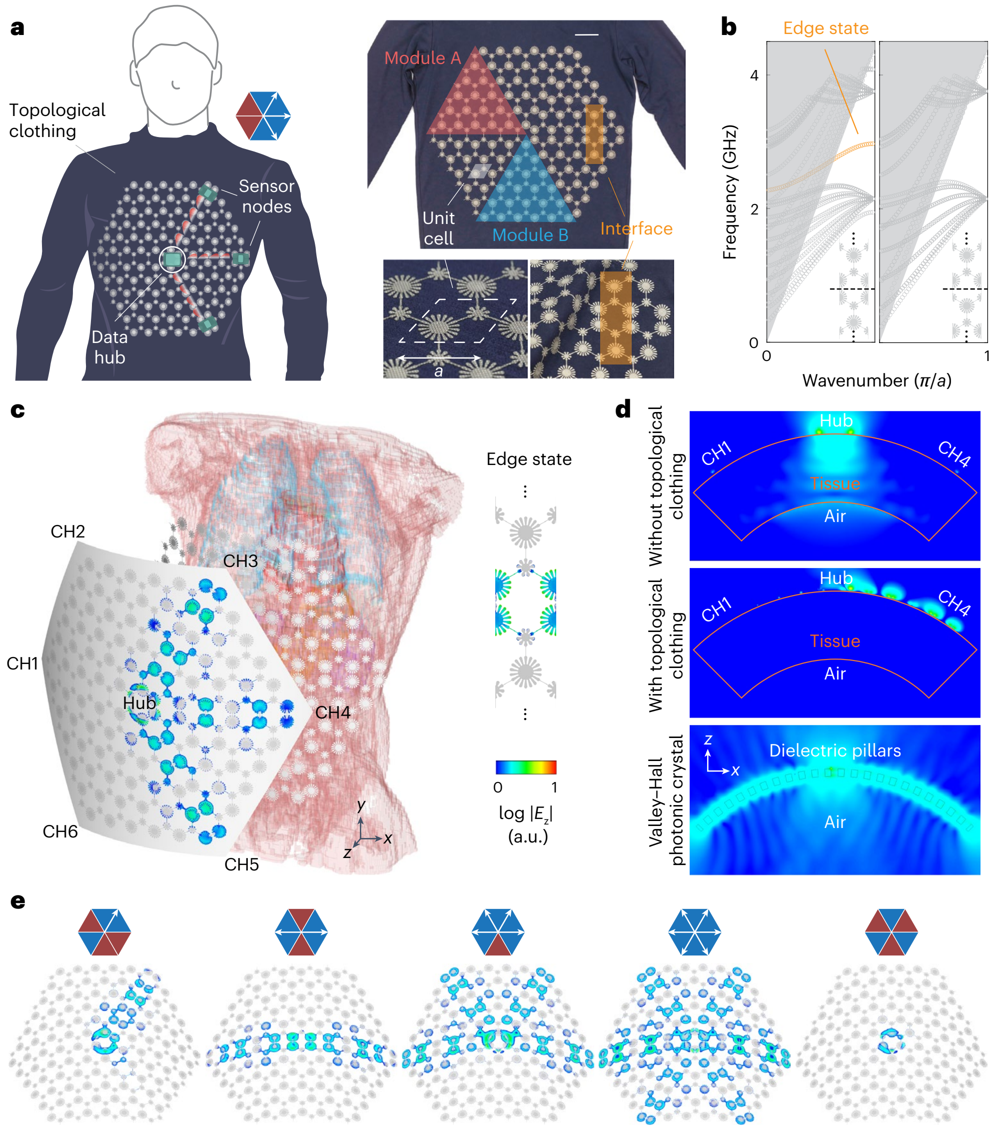

Fig. 1 | Flexible topological clothing on the human body. a, Illustration of topological clothing and interconnected biosensors by topological edge states. The topological clothing consists of two modules (module A, red triangle; module B, blue triangle) with distinct topological phases. The edge state emerges when the two modules are interfaced (yellow shaded area). Inset: the designed wave propagation directions (white arrows). *a*: unit-cell length. Scale bar: 50 mm. **b**, Band structures for different types of interface. The shaded area is the light cone. **c**, Full-wave simulation of topological clothing on a computational human body model. Wireless channels 1–6 are labelled as CH1–6. E_z, electrical field distribution in the *z* direction. **d**, High energy absorption by tissue without topological clothing (top), robust topological edge state on tissue (middle) and high bending loss in conventional topological photonic crystals (bottom). **e**, Modular designs of topological clothing. Electrical field distributions show all the achieved topological clothing with the numbers of topological edge states $n = 1, 2, 4, 6, 0$, respectively.

valley Chern numbers using metallic conductive textiles (Fig. 1a). Wireless links are formed by topological edge states at the interface of two distinct modules, which are located below the light cone in the band diagram (Fig. 1b,c). Unlike conventional topological photonic crystals, the topological edge states in our planar metallic structures manifest as plasmonic surface waves, which reduces bending loss (Fig. 1d).

When conformally attached to the human body, the topological clothing can enhance transmission efficiency by over three orders of magnitude (>30 dB) compared with conventional radiative networks. We show that the topological clothing with interconnected biosensors, and enhanced with machine learning algorithms, can monitor vital signs during exercise with over two orders of magnitude improvement in signal-to-noise ratio (SNR) and a threefold increase in accuracy compared with systems without the topological design. Our modular design also allows reconfiguration by varying the combinations of distinct topological phase modules, offering high design flexibility for diverse on-body applications (Fig. 1e).

System design

Wireless wearable biosensors are essential components in physiological monitoring and modern healthcare systems. Interconnecting these devices across different anatomical regions enables comprehensive mapping of spatially distributed physiological signals on the human body. Conventional wireless body sensor networks rely on electromagnetic fields and over-the-air communication technologies, which are energy-intensive and susceptible to external interception. To address these challenges, electromagnetic surface waves—primarily spoof surface plasmon waves and magneto-inductive waves—have been explored for transmitting signals along the body surface rather than radiating into free space[22–28], thereby improving energy efficiency and data security. However, current implementations of wireless body sensor networks remain limited to one-dimensional electromagnetic waveguides, such as coil relays and spoof surface plasmon channels[22–28]. These designs require different custom components, such as power dividers and circulators, to connect varying numbers of wireless channels. The demonstrated wireless channels and the interconnected sensors are typically limited to three. These systems are thus highly personalized and constrained to narrow application scenarios after the design and fabrication.

We propose topological clothing for modularly designed body sensor networks, as illustrated in Fig. 1. Compared with existing one-dimensional structures, our approach—based on two-dimensional topological modules—offers a higher degree of design flexibility. For instance, with just two topological modules (Fig. 1a), various network configurations can be realized, supporting up to six wireless channels. This modular reconfigurability enables broad adaptability for diverse application scenarios. Figure 1a specifically illustrates flexible topological clothing designed to establish three wireless channels on the human body. Biosensors positioned along these channels capture physiological signals, which are then wirelessly transmitted to a central data hub located at the textile centre. Because wireless signals are confined to the channels and do not radiate into the surrounding space, this design enables efficient, interference-resistant and inherently secure personal sensor networks.

We design topological clothing using a flat valley-Hall topological model—photonic analogues of two-dimensional valleytronic materials that leverage the valley degree of freedom established by lattice symmetry[29–31]. The rhombus unit cell is composed of two flower-shaped resonators supporting spoof surface plasmon resonance (Fig. 2a,b). The lattice constant is $a = 35$ mm, and the radii of the resonators are denoted $r_{1,2}$, respectively. An unpatterned metallic conductor forms the bottom layer of the unit cell. Band diagrams of unit cells with varying dimensions reveal that preserving inversion symmetry ($r_1 = r_2$) results in degenerate Dirac points at K and K′ valleys (Fig. 2c). Breaking inversion symmetry by either $r_1 > r_2$ or $r_1 < r_2$ opens topological bandgaps at K and K′ valleys with opposite-signed valley Chern numbers (Supplementary Notes and Supplementary Fig. 1).

By engineering the unit cells into a honeycomb lattice, we construct two topological modules with distinct topological phases (Fig. 1a and Supplementary Fig. 1): module A ($r_1 = r_2/1.8$) and module B ($r_1 = r_2 \times 1.8$). The interface in Fig. 1b (left) generates a pair of topological edge states governed by the bulk-boundary correspondence principle. These edge states reside within the bandgap and are further visualized in electrical near-field distributions (Fig. 1c). The edge state confines energy to the surface of the topological clothing, allowing it to propagate along the curvature of the tissue (Fig. 1d, middle). This contrasts with the system without topological clothing, where energy penetrates and is absorbed by the tissue (Fig. 1d, top). The edge states extend evanescently in the z direction, enabling contactless excitation in the near field without requiring specialized connectors.

No edge states form between modules of the same topological phases (Fig. 1b and Supplementary Fig. 2), enabling the design of customizable topological clothing with varying numbers of wireless channels by simply combining modules A and B. Figure 1e presents six topological clothing designs with open channel numbers of $n = 0, 1, 2, 3, 4$ and 6, respectively.

Simulations of transmission coefficients and electrical near-fields confirm the high-efficient wireless channels, aligning with the designs (Fig. 1c–e and Supplementary Fig. 3). The topological clothing maintains robust performance under various bending angles or in contact with the human body, with low bending loss, characterized by transmission coefficient degradation, remaining below 2 dB (Supplementary Figs. 4–7). In contrast, conventional topological photonic crystals made from dielectric materials experience high bending loss (~10 dB) when bent out of plane (Supplementary Fig. 4), as energy radiates into the surrounding space under bending (Fig. 1d, bottom). We also notice that precise sensor alignment along the topological channel plays a critical role in achieving such efficient signal transmission (Supplementary Fig. 9).

Compared with existing body sensor network designs, which rely on one-dimensional coil relays or spoof surface plasmon waveguides[22–28], our method using two-dimensional topological modules offers a substantially higher degree of design flexibility (Supplementary Fig. 21). Noted that the interface of modular A–A also generates topological edge states shown in the band diagram (Supplementary Fig. 2). However, due to the small-sized resonators at the interface, the plasmonic coupling is too weak to propagate the wireless signal, causing high asymmetrical propagation (Fig. 1d, middle). This feature further enhances the flexibility of our topological clothing designs, enabling even greater adaptability for diverse applications (Supplementary Fig. 3).

Fabrication and characterization

We fabricate six designed topological structures in Fig. 1 using metallic conductive textiles (Supplementary Fig. 3), which are flexible and stretchable (Supplementary Fig. 12), allowing them to conform seamlessly to the human body. We evaluate the wireless transmission ability of the fabricated topological clothing at the 2.4 GHz industrial, scientific and medical frequency band. Two identical coil antennas, serving as a transmitter and receiver, are placed at the centre of the textile and the end of the wireless channel, respectively (Supplementary Fig. 13). The non-radiative properties of the coil antennas ensure more secure communication localized to the body surface. Although topological metamaterials using metallic materials have been reported[17,32,33], they cannot be directly integrated into clothing due to their three-dimensional structures or high energy dissipation in tissue.

We first measure the electrical near-field distributions of topological clothing with three open channels. Experimental results confirm the presence of three open channels (CH3, CH4 and CH5), which agree well with simulations (Fig. 2a). Transmission coefficients for the open channels are approximately −17 dB, while closed channels exhibit lower transmission at −55 dB (Fig. 2d). The transmission is enhanced by over three orders of magnitude (>30 dB, Fig. 2d) compared with the system without topological clothing. This enhancement is attributable solely to the topological structures, as the transmission coefficients of the bottom layer alone are comparable to radiative methods (Supplementary Fig. 15).

Besides underlying topological physics, the mechanism of open and closed channels could also be understood by the selective propagation of surface plasmon modes. For an array of flower-shaped unit cells made from conductive textiles (Fig. 2b), the surface plasmon dispersion relation (Fig. 2c) determines a bandgap: a certain range of frequencies that cannot be propagated inside the metamaterial, as the metamaterial exhibits high impedance that stops and reflects the electromagnetic fields with frequencies inside the bandgap. However, such a bandgap can be closed by the topological edge state below the light line (Fig. 1b), which propagates the surface plasmon mode with high spatial confinement.

Conventional topological devices typically exhibit performance degradation when bent or integrated with lossy media. To evaluate the robustness of our devices, we subject the topological clothing to bending angles of 10°, 20°, 30°, 40°, 60° and 90° and integrated them with the human body. Transmission spectra for all channels under these conditions demonstrate robust performance with negligible bending loss (Fig. 2e and Supplementary Fig. 15). We also measure the electrical near-field distributions and transmission coefficients of all other fabricated topological clothing with open channel numbers of $n = 1, 2, 4$ and 6 (Fig. 2f). Experimental results align with design expectations and simulations, maintaining resilience to bending and body integration (Supplementary Figs. 4–7).

https://doi.org/10.1038/s41928-025-01516-w

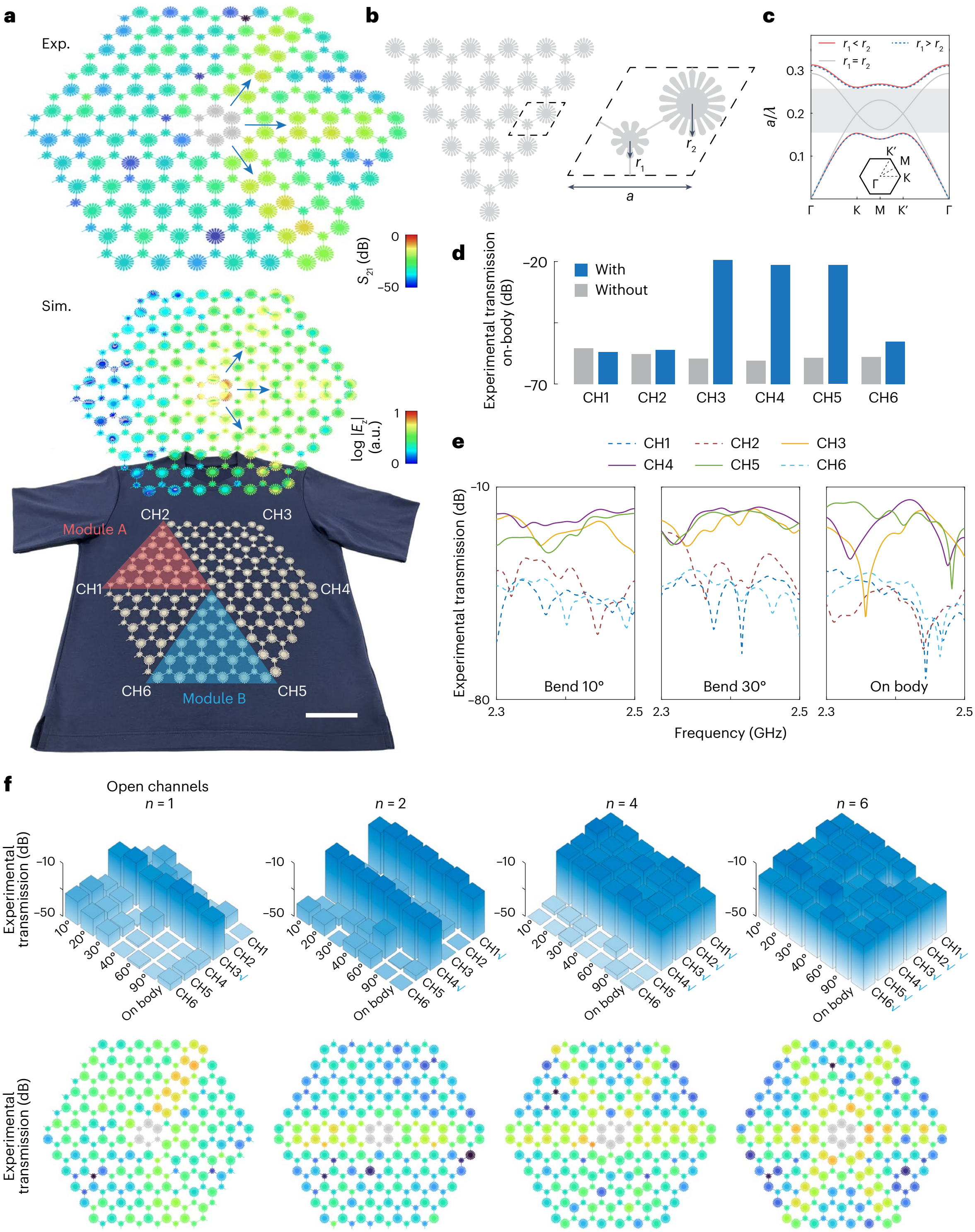

Fig. 2 | Experimental characterization of topological clothing. **a**, Experimental results (Exp.) of electrical field distribution of topological clothing. The results agree well with the simulation (Sim.). S_{21}: transmission coefficient. Scale bar: 60 mm. **b**, Illustration of the topological module, unit cell and its dimensions. a: unit-cell length; $r_{1,2}$, the radius of the left-disc and right-disc shapes. **c**, Band diagrams for the unit cells with $r_1 = r_2/1.8$, $r_1 = r_2 \times 1.8$ and $r_1 = r_2$. The shaded are shows the bandgap. λ, wavelength. **d**, Experimental transmission (trans.) coefficients at 2.4 GHz with and without topological clothing. **e**, Experimental transmission spectra of all the channels when the topological clothing is bent by 10° and 30° and attached to human body. **f**, Experimental transmission coefficients and field distributions at 2.4 GHz (same colour legend as in **a**). The topological clothing with open channels n = 1, 2, 4 and 6 are bent with angles of 10°, 20°, 30°, 40°, 60° and 90°, and attached to the human body.

We next evaluate the ability of topological clothing to enhance wireless signal transmission between body-worn devices. Figure 3a shows topological clothing with three open channels (n = 3) used to interconnect commercial Bluetooth devices functioning as wireless biosensors on a human participant. A Bluetooth dongle connected to a laptop records the relative signal strength indicator (RSSI) from six channels. These Bluetooth devices use coil antennas to better confine electromagnetic fields to the body surface. We conduct real-time RSSI

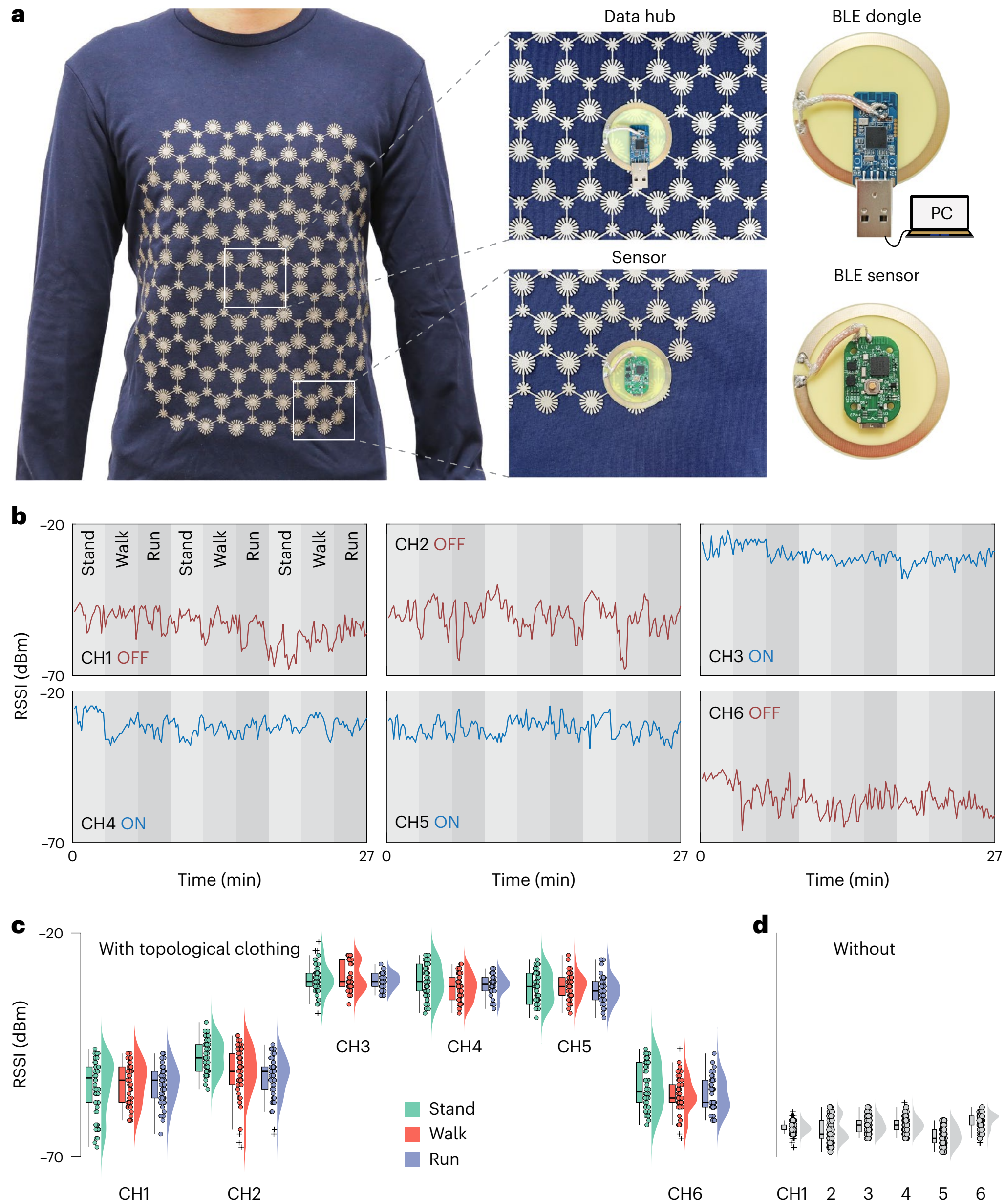

Fig. 3 | Experimental characterization of enhanced wireless communication on the body during exercise. a, Wireless network of Bluetooth devices on the body. Six sensors are placed at the end of six channels, and a data hub is placed on the centre of topological clothing to measure RSSI from all six channels. BLE, Bluetooth low energy. **b**, The recorded RSSI data from six channels during exercise in 27 min. **c**, Violin plots of the measured RSSI in the six channels during the exercise statuses of standing, walking and running. The centre line inside the violin plot represents the median, the box edges mark the interquartile range (25th–75th percentiles) and the whiskers extend to the minimum and maximum values within 1.5 times the interquartile range. **d**, The RSSI and violin plots for the comparison study without the topological clothing. **c** and **d** represent multiple contemporary measurements (162 and 120 samples, respectively) from the same experiments.

monitoring with a healthy volunteer wearing a central hub and six sensors during a simulated daily activity protocol comprising alternating 3-minute intervals of standing, walking and running, repeated three times. As a control, the activity protocol is repeated using a conventional over-the-air communication network without the topological clothing (Supplementary Fig. 14).

Figure 3b presents RSSI data over 27 min of standing, walking and running. Violin plots in Fig. 3c show minimal RSSI variation (<2 dB) across activities, highlighting the robust wireless communication capabilities of the topological clothing in high-noise scenarios. The RSSI difference between open and closed channels is ~25 dB, allowing efficient connection with the desired sensors while disconnecting unwanted ones. Compared with conventional wireless networks without topological clothing—while keeping the transceiver antennas identical—the RSSI is enhanced by more than 40 dB (Fig. 3d). These improvements translate to reduced power consumption, increased data throughput and extended battery life for wireless biosensors.

Sensitive vital-sign monitoring

The measurement of vital signs, including respiration and heartbeat, is essential for monitoring a wide range of physiological conditions, such as hypoxia, hypercapnia, metabolic acidosis and physical exertion during exercise[34]. Wearable accelerometers, gyrosensors and magnetometers placed on the torso can unobtrusively register respiratory and heartbeat motion[35]. However, these sensors are inherently susceptible to noise introduced by non-respiratory and non-cardiac motions,

https://doi.org/10.1038/s41928-025-01516-w

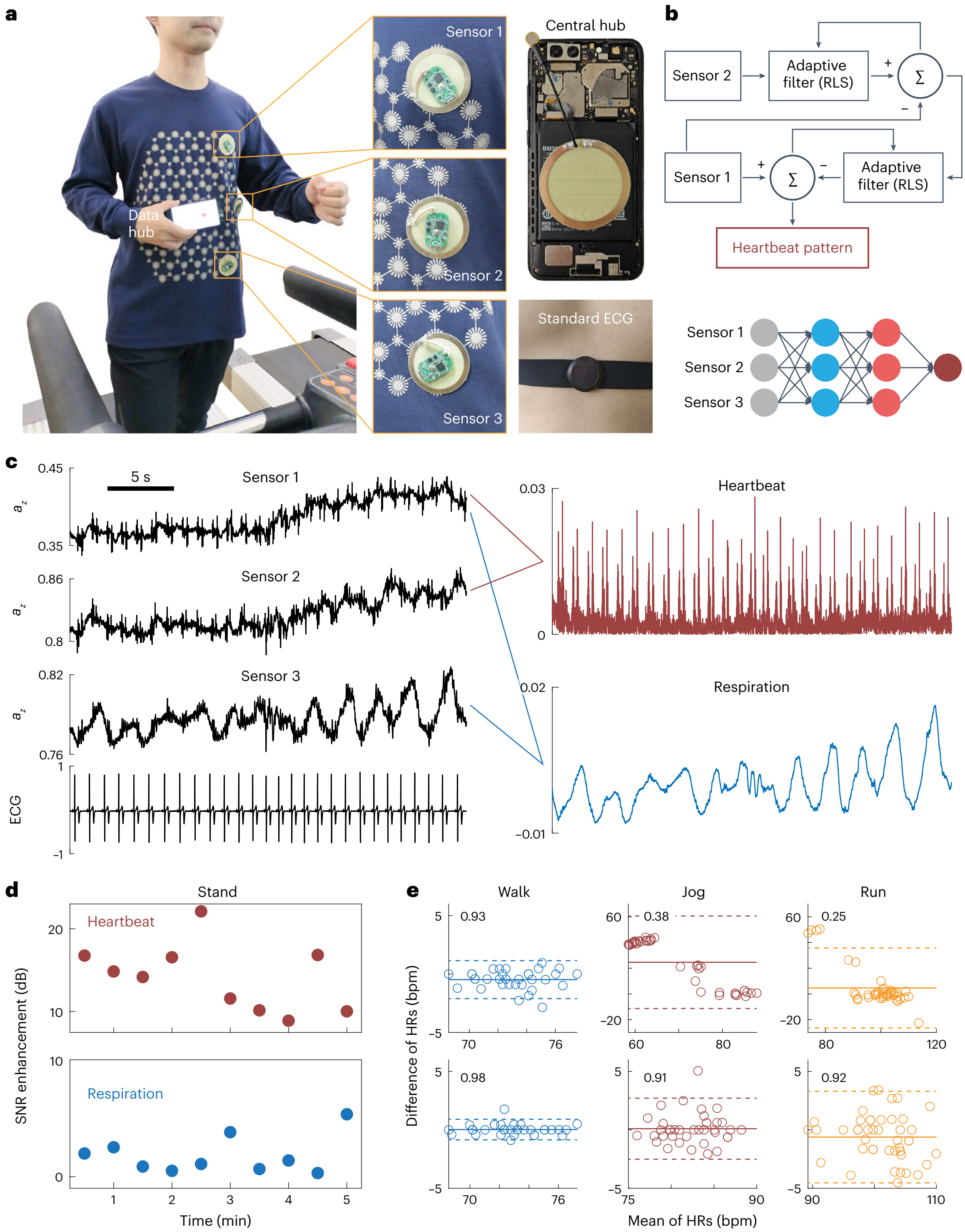

Fig. 4 | Demonstration of sensitive vital-sign monitoring during exercise. **a**, Three Bluetooth accelerometers placed on topological clothing and worn on the body. A smartphone is placed on the centre as the data hub. An on-skin ECG sensor is used as a reference signal. **b**, Two algorithms for exercise data processing. A two-step adaptive filter is used to obtain clean heartbeat and respiration patterns when the participant is still, and a recurrent neural network algorithm is used for walking, jogging and running statuses. RLS, recursive least-squares. **c**, Sample data from four sensors (left) and processed heartbeat and respiration patterns (right) in the first 30-second window of stand status. **d**, SNR enhancements in detecting heart rates (HRs) and respiration rates. **e**, Bland–Altman plots of measured HRs using machine intelligence algorithms and data from single-sensor node (top) and sensor network (bottom). Pearson correlation coefficients of measured HRs are listed within the plot. Data are obtained from multiple contemporary measurements from the same participant, which are represented as mean (solid line) ± 1.96 × s.d. (dashed lines). Sample sizes for walk, jog and run are 34, 38 and 44, respectively.

leading to low SNR and reduced accuracy compared with clinical-grade instruments, particularly during exercise and daily activity[36]. Many approaches have been proposed to suppress motion noise, including the use of soft materials to reduce random mechanical variability and machine learning algorithms to remove motion artefacts[37,38]. In circuit design, differential strategies combined with machine learning algorithms are commonly used to mitigate motion interference[39–41]. However, these methods typically rely on a single device to collect differential signals from a limited body region, resulting in lower signal contrast.

We demonstrate the capability of our topological clothing to mitigate noise in a wireless network of accelerometers unobtrusively worn on the body. Figure 4a illustrates the experimental setup, where a participant performs a treadmill protocol consisting of standing, walking, jogging and running at incremental speeds of 0 km h^{-1}, 1 km h^{-1}, 3 km h^{-1} and 5 km h^{-1}. respectively, with each phase lasting 5 minutes. Three accelerometers, placed on the chest, abdomen and lower abdomen, record motions induced respiration and heartbeat. The accelerometer data along the z axis are wirelessly transmitted to a central hub (smartphone) on the abdomen via coil antennas. These devices are interconnected through the edge states of the topological clothing, ensuring energy-efficient and secure communication. A clinical-grade electrocardiogram (ECG) monitor provides reference measurements of respiration and heartbeat (Supplementary Fig. 13).

Figure 4c shows acceleration data from the three sensors alongside standard ECG signals during the first 30-second still phase. The complete dataset of the 27-minute exercise protocol is provided in Supplementary Fig. 17. The chest accelerometer exhibits pronounced motion artefacts and stronger heartbeat components, while the lower abdomen accelerometer predominantly captures respiratory patterns. To extract cleaner signals, we apply a two-step adaptive filtering algorithm that leverages data from all three accelerometers[41] (Fig. 4b). Using z-axis accelerations from the chest and abdomen sensors, we isolate a cleaner heartbeat signal with distinct vibration (V) peaks, matching the R peaks in the ECG signal, apart from a minor time delay (Fig. 4c). Respiration patterns are clarified by processing data from the abdomen and lower abdomen sensors through the same adaptive filters (Supplementary Fig. 18).

To quantify the performance enhancement achieved with the topological clothing, we calculate the SNR for the detected respiration rate and heart rate. The SNR from a single accelerometer placed on the chest or lower abdomen serves as the baseline for heartbeat and respiration monitoring, respectively. Figure 4d reveals SNR improvements, with heart rate detection SNR increasing by up to 158-fold (22 dB) and respiration rate detection SNR improving by 2.4-fold (3.8 dB). These results highlight the capability of topological clothing to amplify weak bio-signals, such as heartbeats, by more than two orders of magnitude. The time-varying SNR in our approach is due to the random motion noise (Supplementary Fig. 19). Other signal-processing algorithms, including Butterworth and Kalman filters[42,43], could further enhance SNRs, making the system even more effective for precise vital-sign monitoring.

We also use artificial intelligence algorithms to extract heart rate during high-noise activities of walking, jogging and running. A long short-term memory (LSTM) model is trained using input from all three accelerometers in the wireless network. Controls with a single-sensor node input and the same LSTM model are performed for comparison. The accuracy is evaluated using Bland–Altman plots and Pearson correlation coefficients (Fig. 4e). The topological clothing-based sensor network maintains high accuracy across all activities despite increasing motion noise, whereas single-sensor performance deteriorates during jogging and running (Supplementary Fig. 20). Notably, heart rate detection accuracy improves by 3.7-fold with the topological clothing during running.

Conclusions

We have reported topological devices that interact with the human body. We fabricated thin topological clothing using metallic conductive textiles, addressing the challenges of low flexibility and high energy loss in integrating topological photonic devices with the human body. Our topological body sensor networks enhance signal transmission on the human body by over three orders of magnitude compared with conventional radiative networks. We also showed that multiple biosensors interconnected by our topological clothing can provide sensitive vital signs monitoring during exercise, achieving improvements of over two orders of magnitude in SNR and a threefold increase in detection accuracy compared with systems without the topological design. Our work bridges the fields of topological physics and biological systems[44,45], providing a starting point for translating photonic concepts—such as topological insulators and bound states in the continuum[46–48]—into biomedical applications.

Methods

Numerical simulations

Electromagnetic simulations were carried out with CST Microwave Studio (Dassault Systems). The band structures of the unit cells were obtained by solving the eigenfrequencies within the hexagonal Brillouin zone using the Eigenmode Solver. Field distributions were calculated using the finite-integration technique in the time-domain method. The conductive textile was assigned as perfect electric conductor in simulations. The computational body model used an anatomically accurate voxel model (Hugo, CST Voxel Family) with a resolution of 1.875 × 1.875 × 1.25 mm. Coil antennas and discrete ports were used to transmit and receive wireless signals. In the body simulation, the topological clothing was bent by 90° and in proximity to the human body.

Textile fabrications

Conductive textile patterns were laser-cut (Universal Laser Systems, VLS 2.30) from adhesive Cu/Ni polyester fabric sheets (Conductive Fabric Tape 86750, Laird Technologies; Conductive Non-woven Fabric 4770, Holland Shielding Systems). Patterns were attached to a cotton–polyester blend athletic shirt for radio-wave devices and wireless communication experiments. When worn on the body, the body bends the topological metamaterial by about 90°.

To ensure strong adhesion between the conductive textile and the clothing, a three-step process is used. First, a layer of heat-adhesive film is placed onto the conductive fabric and bonded using a Hot Press. Second, the conductive fabric with the adhesive layer is patterned with a laser cutter. The conductive fabric is flexible and has a Young's modulus compatible with the underlying clothing. Third, the patterned fabric is positioned on the clothing with the adhesive side facing down and permanently affixed by pressing again with a heat press. These steps ensure that the topological structures are tightly attached to the clothing, remaining robust under scratching and everyday handling.

Consideration of the carbon footprint during textile fabrications

The carbon footprint of the topological clothing is minimized by optimizing the number of unit cells, fabrication resolution and tolerance to defects. Simulations (Supplementary Fig. 10) confirm that only periods of flower-shaped resonators near the topological edge are sufficient for waveguiding, reducing material use and fabrication time. A spatial resolution of 0.15 mm ensures strong field confinement while enabling energy-efficient, low-precision laser cutting (Supplementary Fig. 8). In addition, simulations with random defects (Supplementary Fig. 11) show the structure remains robust and high transmission coefficients, effectively tolerating small fabrication imperfections. These strategies collectively support sustainable, low-carbon manufacturing of topological metamaterials.

Transmission and field measurements

Transmission was measured as |S21| between two identical coil antennas with a 4.5 cm diameter connected to a vector network analyser (N9915A, Keysight) using coaxial cables (SMA-SMA, 50Ω, Amphenol). One coil antenna was placed on the centre of the topological clothing and the other one was placed on the end of each edge channel. The coil antenna was designed to optimally cover the near-field region at the end of the channel. The coil antenna features a low gain of 1.751 dBi, minimizing the transmission of information into free space.

Due to the vector network analyser's port limitation, measurements were performed sequentially for each wireless channel, with other channels left open. To evaluate the impact of sensor deployment, we compared two configurations: (1) a single-sensor load connected to one wireless channel, and (2) six sensor loads connected simultaneously to six different channels. Each sensor load consisted of a coil antenna terminated with a 50-Ω resistor to emulate a typical sensor impedance. For the multi-load configuration, only one channel was measured at a time while the remaining five channels were loaded. The results, both numerical and experimental, show that the presence of multi-sensor loads has minimal influence on the transmission coefficients (Supplementary Fig. 16).

Field mapping experiments used a probe mounted on a three-dimensional positioning system. The source used a coil antenna placed 2 mm above the input position on the centre of the textile. The probe used the same coil antenna and scanned 5 mm above each localized-surface-plasmon resonators. Signals from the probe were measured by a vector network analyser (N9915A, Keysight).

RSSI measurements

Evaluation of topological clothing on the body was performed with a healthy participant recruited from the National University of Singapore. All participants were volunteers and provided informed consent. RSSI measurements were performed using the Bluetooth low energy protocol. Sensor nodes made use of single-mode Bluetooth v.4.0 modules (nRF52832) configured with a self-customized coil antenna and a 130 mAh lithium battery. Sensors were transmitted to a central hub using a nRF52840 Dongle connected to a PC, running a connectivity application (nRF Connect for Desktop, Nordic Semiconductor) that recorded the signal strength. The sensors were placed at the end of each channel and the Bluetooth low energy dongle was placed on the centre of the topological clothing. The central data hub recorded the received signal strength during indoor physiological activity (standing, walking and running) in 3-min trials and repeated 3 times. Controls were performed by repeating the 2-min activity protocol with an unpatterned athletic shirt.

Vital-sign monitoring

Vital-sign monitoring was performed with a healthy participant from National University of Singapore. All participants were volunteers and provided informed consent. Three accelerometers (MPU-9250) were placed on the end of the three open channels of the topological clothing and worn on the body. Sensors were transmitted to a central hub consisting of an Android smartphone configured with a self-customized coil antenna running a connectivity application (nRF Connect, Nordic Semiconductor). The activity protocol of standing (0 km h^{-1}), walking (1 km h^{-1}), jogging (3 km h^{-1}) and running (5 km h^{-1}) were conducted in 20 min. Physiological experiments complied with a protocol approved by the National University of Singapore.

Two-step adaptive filtering algorithm

The two-step adaptive filtering algorithm was adopted from ref. 36. In the first adaptive filtering, the motion noise signal was extracted by subtracting the chest acceleration signal from that of the lower abdomen acceleration signal. In the second adaptive filtering, the heartbeat pattern was obtained by subtracting the motion noise signal, extracted by the first adaptive filtering, from that of the chest accelerometer. These processes used the recursive least-squares adaptive filter provided in MATLAB at each adaptive filtering step. The respiration pattern was obtained using the same two-step adaptive filtering algorithm using the acceleration signals from the chest and the lower abdomen. Recursive least-squares filtering parameters involved a filter length of 3 taps and 30 taps for respiration and heartbeat, respectively, and a forgetting factor of 0.98. The SNR was evaluated by dividing the output signal into 30-s windows. In each window, a fast Fourier transform was performed, and the SNR was calculated as $10\log_{10}(S(\Omega)/N_0)$, where $S(\Omega)$ is the power spectrum density at the respiratory rate Ω and N_0 is power spectral density averaged across all frequencies except Ω.

Artificial neural networks

A LSTM model was used to measure heart rate during high-noisy activities including walking, jogging and running. Before the training of the model, we preprocessed the data: standardization was used to scale the features and labels, and the data were filtered to ensure the stability of the model training. To ensure the accuracy and stability of prediction, we screened and predicted the extreme point with an ECG signal greater than 0.4 and less than −0.4. To predict the large and small waveforms in a heartbeat signal, we screened and predicted the points with an ECG signal greater than 0.1 and less than −0.1. The entire network consisted of multiple LSTM layers and fully connected layers (dense layer), which were serialized by adding activation functions (such as rectified linear units) and batch normalization layers between each adjacent layer. During the training process of the model, the difference between the mean absolute error) was calculated as the loss function. To avoid overfitting, the network used a Dropout layer to randomly discard some of the neurons. To optimize the training process, we used learning rate attenuation and early stop (EarlyStopping) techniques to ensure that the training process is more stable and to avoid overfitting caused by excessive training. After the training, an independent set of test data were used to evaluate the prediction accuracy of the trained LSTM model, and the mean square error and R^2 values of the model were calculated to further measure the performance of the model. The heart rate was finally calculated based on the time difference of adjacent local maxima using find_peaks function in the scipy.signal module.

Reporting summary

Further information on research design is available in the Nature Portfolio Reporting Summary linked to this article.

Data availability

The data that support the plots within this paper are available via GitHub at https://github.com/zhipengli-ustc/body_sensor_network_topological_clothing. Source data are provided with this paper.

Code availability

The codes are available via GitHub at https://github.com/zhipengli-ustc/body_sensor_network_topological_clothing.

References

1. Hasan, M. Z. & Kane, C. L. Colloquium: topological insulators. *Rev. Mod. Phys.* **82**, 3045 (2010).
2. Lu, L., Joannopoulos, J. D. & Soljacic, M. Topological photonics. *Nat. Photonics* **8**, 821 (2014).
3. Ozawa, T. et al. Topological photonics. *Rev. Mod. Phys.* **91**, 015006 (2019).
4. Krishnamoorthy, H. N. S., Dubrovkin, A. M., Adamo, G. & Soci, C. Topological insulator metamaterials. *Chem. Rev.* **123**, 4416 (2023).
5. Kim, M., Jacob and, Z. & Rho, J. Recent advances in 2D, 3D and higher-order topological photonics. *Light.: Sci. Appl.* **9**, 130 (2020).
6. You, J. W. et al. Topological metasurface: from passive toward active and beyond. *Photonics Res.* **11**, B65 (2023).
7. Zhang, X., Z.-Nejad, F., Chen, Z.-G., Lu, M.-H. & Chirstensen, J. A second wave of topological phenomena in photonics and acoustics. *Nature* **618**, 687 (2023).
8. Khanikaev, A. B. et al. Photonic topological insulators. *Nat. Mater.* **12**, 233 (2013).
9. Liu, Z. et al. Topological thermal transport. *Nat. Rev. Phys.* **6**, 554 (2024).

10. Xue, H., Yang, Y. & Zhang, B. Topological acoustics. *Nat. Rev. Mater.* **7**, 974 (2022).
11. Shankar, S., Souslov, A., Bowick, M. J., Marchetti, M. C. & Vitelli, V. Topological active matter. *Nat. Rev. Phys.* **4**, 380 (2022).
12. Yang, Y. et al. Terahertz topological photonics for on-chip communication. *Nat. Photonics* **14**, 446 (2020).
13. Shalaev, M. I., Walasik, W., Tsukernik, A., Xu, Y. & Litchinitser, N. M. Robust topologically protected transport in photonic crystal at telecommunications wavelengths. *Nat. Nanotechnol.* **14**, 31 (2019).
14. Bahari, B. et al. Nonreciprocal lasing in topological cavities of arbitrary geometries. *Science* **358**, 636 (2017).
15. Barik, S. et al. A topological quantum optics interface. *Science* **359**, 666 (2018).
16. Wang, W. et al. On-chip topological beamformer for multi-link terahertz 6G to XG wireless. *Nature* **632**, 522 (2024).
17. Gao, Z., Gao, F., Zhang, Y., Luo, Y. & Zhang, B. Flexible photonic topological insulators. *Adv. Opt. Mater.* **6**, 1800532 (2018).
18. Rosiek, C. A. et al. Observation of strong backscattering in valley-Hall photonic topological interface modes. *Nat. Photonics* **17**, 386 (2023).
19. Li, Z., Tian, X., Qiu, C.-W. & Ho, J. S. Metasurfaces for bioelectronics and healthcare. *Nat. Electron.* **4**, 382 (2021).
20. Negra, R., Jemili, I. & Belghith, A. 'Wireless body area networks: applications and technologies. *Procedia Comput. Sci.* **83**, 1274 (2016).
21. Niu, S. et al. A wireless body area sensor network based on stretchable passive tags. *Nat. Electron.* **2**, 361 (2019).
22. Tian, X. et al. Wireless body sensor networks based on metamaterial textiles. *Nat. Electron.* **2**, 243 (2019).
23. Lin, R. et al. Wireless battery-free body sensor networks using near-field-enabled clothing. *Nat. Commun.* **11**, 444 (2020).
24. Lin, R. et al. Digitally-embroidered liquid metal electronic textiles for wearable wireless systems. *Nat. Commun.* **13**, 2190 (2022).
25. Tian, X. et al. Implant-to-implant wireless networking with metamaterial textiles. *Nat. Commun.* **14**, 4335 (2023).
26. Hajiaghajani, A. et al. Textile-integrated metamaterials for near-field multibody area networks. *Nat. Electron.* **4**, 808 (2021).
27. Zhu, X., Wu, K., Xie, X., Anderson, S. W. & Zhang, X. A robust near-field body area network based on coaxially-shielded textile metamaterial. *Nat. Commun.* **15**, 6589 (2024).
28. Yuce, M. R. Implementation of wireless body area networks for healthcare systems. *Sens. Actuators A* **162**, 116 (2010).
29. Duan, X. et al. Valley-addressable monolayer lasing through spin-controlled Berry phase photonic cavities. *Science* **381**, 1429 (2023).
30. Zeng, Y. et al. Electrically pumped topological laser with valley edge modes. *Nature* **578**, 246 (2020).
31. He, X.-T. et al. A silicon-on-insulator slab for topological valley transport. *Nat. Commun.* **10**, 872 (2019).
32. You, J. W. et al. Reprogrammable plasmonic topological insulators with ultrafast control. *Nat. Commun.* **12**, 5468 (2021).
33. Ma, Q. et al. Observation deformation-induced backscattering in flexible valley-Hall topological metasurfaces. *Adv. Opt. Mater.* **13**, 2402078 (2024).
34. AL-Khalidi, F. Q., Saatchi, R., Burke, D., Elphick, H. & Tan, S. Respiration rate monitoring methods: a review. *Pediatr. Pulmonol.* **46**, 523 (2011).
35. Yoon, J.-W., Noh, Y.-S., Kwon, Y.-S., Kim, W.-K. & Yoon, H.-R. Improvement of dynamic respiration monitoring through sensor fusion of accelerometer and gyro-sensor. *J. Electr. Electron. Eng. Technol.* **9**, 334 (2014).
36. Jeong, H. et al. Differential cardiopulmonary monitoring system for artifact-canceled physiological tracking of athletes, workers, and COVID-19 patients. *Sci. Adv.* **7**, eabg3092 (2021).
37. Meng, K. et al. Kirigami-inspired pressure sensors for wearable dynamic cardiovascular monitoring. *Adv. Mater.* **34**, 2202478 (2022).
38. Lee, S. H. et al. Fully portable continuous real-time auscultation with a soft wearable stethoscope designed for automated disease diagnosis. *Sci. Adv.* **8**, eabo5867 (2022).
39. Chen, S. et al. Starfish-inspired wearable bioelectronic systems for physiological signal monitoring during motion and real-time heart disease diagnosis. *Sci. Adv.* **11**, eabe1655 (2020).
40. Park, Y. et al. Wireless, skin-interfaced sensors for compression therapy. *Sci. Adv.* **6**, eadv2406 (2025).
41. Yoo, J. Y. et al. Wireless broadband acousto-mechanical sensing system for continuous physiological monitoring. *Nat. Med.* **29**, 3137 (2023).
42. Estrada, L., Torres, A., Sarlabous, L. & Jane, R. Respiratory signal derived from the smartphone built-in accelerometer during a respiratory load protocol. In *Proc. 2015 37th Annual International Conference of the IEEE Engineering in Medicine and Biology Society (EMBC)*, 6768 (IEEE, 2015).
43. Vertens, J. et al. Measuring respiration and heart rate using two acceleration sensors on a fully embedded platform. In *Proc. 3rd International Congress on Sport Sciences Research and Technology Support (icSPORTS 2015)*, Vol. 1 (eds Cabri, J. & Pezarat Correia, P.) 15–23 (SciTePress–Science and Technology Publications, 2015).
44. Zaky, Z. A. et al. Coupling between topological edge state and defect mode-based biosensor using phononic crystal. *Sci. Rep.* **15**, 2216 (2025).
45. Kong, Z.-L., Liu, Y. & Jiang, J.-H. Topologically integrated photonic biosensor circuits. *Laser Photonics Rev.* **19**, 2401209 (2025).
46. Zhang, Y. et al. Realization of photonic *p*-orbital higher-order topological insulators. *eLight* **3**, 5 (2023).
47. Wang, M. et al. Spin-orbit-locked hyperbolic polariton vortices carrying reconfigurable topological charges. *eLight* **2**, 12 (2022).
48. Chen, Z. & Segev, M. Highlighting photonics: looking into the next decade. *eLight* **1**, 2 (2021).

Acknowledgements

H.J. acknowledges the support from the National Key R&D Program (Grant No. 2024YFE0102400), the National Natural Science Foundation of China (Grant Nos. 11935006 and 12421005) and the Hunan Major Sci-Tech Program (Grant No. 2023ZJ1010). Z. Liu acknowledges the support from Natural Science Foundation of Hunan Province of China (Grant No. 2025JJ50393), The Key Research and Development Program of Hunan Province (Grant No. 2023GK2009), Hunan Provincial Major Sci-Tech Program (Grant No. 2023ZJ1010) and Education Department of Hunan Province of China (Grant No. 24B0059). C.W.Q. acknowledges the support from Ministry of Education, Singapore (Grant No. A-8002152-00-00). We acknowledge the fabrication support from Changsha Multilayer PCB Technology Co., Ltd.

Author contributions

Z. Li, Z. Liu and C.-W.Q. conceived and planned the research. Z. Li, Z. Liu, H.J., J.S.H. and C.-W.Q. designed the wireless systems and performed the simulations. Z. Liu, Y.D., Z.W., Q.Z. and G.L. characterized the system and performed the experiments. Z. Li, S.Y., J.C., Y.Z., H.Y., Z.X., X.T. and Y.C. analysed data and plotted figures. Z. Li and Z. Liu wrote the paper with input from all the authors. C.-W.Q. supervised the project.

Competing interests

The authors declare no competing interests.

Additional information

Supplementary information The online version contains supplementary material available at https://doi.org/10.1038/s41928-025-01516-w.

Correspondence and requests for materials should be addressed to Zhu Liu, Hui Jing or Cheng-Wei Qiu.

Peer review information *Nature Electronics* thanks Jingna Mao and the other, anonymous, reviewer(s) for their contribution to the peer review of this work.

Reprints and permissions information is available at www.nature.com/reprints.

Publisher's note Springer Nature remains neutral with regard to jurisdictional claims in published maps and institutional affiliations.

[1]School of Microelectronics, University of Science and Technology of China, Hefei, China. [2]Department of Electrical and Computer Engineering, National University of Singapore, Singapore, Singapore. [3]Key Laboratory of Low-Dimensional Quantum Structures and Quantum Control of Ministry of Education, Key Laboratory of Physics and Devices in Post-Moore Era, College of Hunan Province, Hunan Research Center of the Basic Discipline for Quantum Effects and Quantum Technologies, School of Physics and Electronics, Hunan Normal University, Changsha, China. [4]Institute of Flexible Electronics (IFE) and Frontiers Science Center for Flexible Electronics, Northwestern Polytechnical University, Xi'an, China. [5]Wireless and Smart Bioelectronics Laboratory, School of Biomedical Engineering, ShanghaiTech University, Shanghai, China. [6]Tsinghua Shenzhen International Graduate School, Tsinghua University, Shenzhen, China. [7]College of Electrical and Information Engineering, Hunan University, Changsha, China. [8]Chinese Academy of Sciences Key Laboratory of Mechanical Behavior and Design of Materials, Department of Precision Machinery and Precision Instrumentation, University of Science and Technology of China, Hefei, China. [9]These authors contributed equally: Zhipeng Li, Zhu Liu. ✉e-mail: zhu_liu@hnu.edu.cn; jinghui@hunnu.edu.cn; chengwei.qiu2@nus.edu.sg

nature portfolio

Corresponding author(s): Cheng-Wei Qiu

Last updated by author(s): Sep 11, 2025

Reporting Summary

Nature Portfolio wishes to improve the reproducibility of the work that we publish. This form provides structure for consistency and transparency in reporting. For further information on Nature Portfolio policies, see our Editorial Policies and the Editorial Policy Checklist.

Statistics

For all statistical analyses, confirm that the following items are present in the figure legend, table legend, main text, or Methods section.

n/a	Confirmed	
☐	☒	The exact sample size (*n*) for each experimental group/condition, given as a discrete number and unit of measurement
☐	☒	A statement on whether measurements were taken from distinct samples or whether the same sample was measured repeatedly
☒	☐	The statistical test(s) used AND whether they are one- or two-sided *Only common tests should be described solely by name; describe more complex techniques in the Methods section.*
☒	☐	A description of all covariates tested
☒	☐	A description of any assumptions or corrections, such as tests of normality and adjustment for multiple comparisons
☐	☒	A full description of the statistical parameters including central tendency (e.g. means) or other basic estimates (e.g. regression coefficient) AND variation (e.g. standard deviation) or associated estimates of uncertainty (e.g. confidence intervals)
☒	☐	For null hypothesis testing, the test statistic (e.g. F, t, r) with confidence intervals, effect sizes, degrees of freedom and P value noted *Give P values as exact values whenever suitable.*
☒	☐	For Bayesian analysis, information on the choice of priors and Markov chain Monte Carlo settings
☒	☐	For hierarchical and complex designs, identification of the appropriate level for tests and full reporting of outcomes
☐	☒	Estimates of effect sizes (e.g. Cohen's d, Pearson's r), indicating how they were calculated

Our web collection on statistics for biologists contains articles on many of the points above.

Software and code

Policy information about availability of computer code

Data collection	Electromagnetic simulations used the finite-difference time-domain method using commercial software (CST Microwave Studio, Dassault Systems). Data collection was perform with open-source software nRF Connect for Desktop.
Data analysis	The data was analyzed with MATLAB R2021a.

For manuscripts utilizing custom algorithms or software that are central to the research but not yet described in published literature, software must be made available to editors and reviewers. We strongly encourage code deposition in a community repository (e.g. GitHub). See the Nature Portfolio guidelines for submitting code & software for further information.

Data

Policy information about availability of data

All manuscripts must include a data availability statement. This statement should provide the following information, where applicable:

- Accession codes, unique identifiers, or web links for publicly available datasets
- A description of any restrictions on data availability
- For clinical datasets or third party data, please ensure that the statement adheres to our policy

The data that support the plots within this paper are available from GitHub at https://github.com/zhipengli-ustc/body_sensor_network_topological_clothing. All other data that support the findings of this study are available within the article and supplementary materials.

Research involving human participants, their data, or biological material

Policy information about studies with human participants or human data. See also policy information about sex, gender (identity/presentation), and sexual orientation and race, ethnicity and racism.

Reporting on sex and gender	N/A
Reporting on race, ethnicity, or other socially relevant groupings	N/A
Population characteristics	Participants in the experiments were healthy subjects.
Recruitment	The participant were recruited by the National University of Singapore (aged 20 to 35). The were no self-selection biases or other biases.
Ethics oversight	All experiments complied with a protocol approved by the National University of Singapore Institutional Review Board (NUS-IRB-2022-561). All subjects were volunteers, were informed of risks and benefits, and provided informed consent.

Note that full information on the approval of the study protocol must also be provided in the manuscript.

Field-specific reporting

Please select the one below that is the best fit for your research. If you are not sure, read the appropriate sections before making your selection.

☒ Life sciences ☐ Behavioural & social sciences ☐ Ecological, evolutionary & environmental sciences

For a reference copy of the document with all sections, see nature.com/documents/nr-reporting-summary-flat.pdf

Life sciences study design

All studies must disclose on these points even when the disclosure is negative.

Sample size	2 healthy subjects were recruited for the evaluation of the sensor.
Data exclusions	No data were excluded from analysis.
Replication	All attempts at replication were successful. The device was used for 2 subjects in different experimental setup.
Randomization	The device was tested in all participants. Randomization was therefore not relevant to the study.
Blinding	Blinding was not relevant to our experiments since the blinding would not influence the results.

Reporting for specific materials, systems and methods

We require information from authors about some types of materials, experimental systems and methods used in many studies. Here, indicate whether each material, system or method listed is relevant to your study. If you are not sure if a list item applies to your research, read the appropriate section before selecting a response.

Materials & experimental systems

n/a	Involved in the study	
☒	☐	Antibodies
☒	☐	Eukaryotic cell lines
☒	☐	Palaeontology and archaeology
☒	☐	Animals and other organisms
☒	☐	Clinical data
☒	☐	Dual use research of concern
☒	☐	Plants

Methods

n/a	Involved in the study	
☒	☐	ChIP-seq
☒	☐	Flow cytometry
☒	☐	MRI-based neuroimaging

Plants

Seed stocks	N/A
Novel plant genotypes	N/A
Authentication	N/A